In search for phase transitions in Casimir force between percolating metal lattices

Michael Flynn, Andrei Klishin, Prashanth Venkataram, Charles Xu*
MIT Department of Physics
(Dated: May 17, 2014)

We provide a derivation of the percolation threshold for a two-dimensional triangular lattice. We then proceed to model an ensemble of skewed square lattices with randomly punched out squares, which is topologically equivalent to triangular lattice percolation. We investigate the behavior of the magnitude of the Casimir force between the percolating plate and the solid plate. We find evidence which suggests that connectivity of the percolating plate has an effect on the long wavelength current excitations on the surface of the conductors and consequently on the magnitude of the Casimir force.

I. INTRODUCTION

The phenomenon of percolation is widely studied in literature. Percolation is a phenomenon of formation of joined networks by random placement of nodes or bonds. Percolation-type phenomena arise in a wide variety of circumstances such as formation of pores in a membrane, or random connection of nodes with resistors in an electric network. Percolation is characterized by existence of a threshold value of the controlling parameter (percolation probability), above which an infinite connected cluster of individual nodes forms in the system.

The most important order parameter of a percolation network is the characteristic size of connected clusters and the probability distribution of this size. The behavior of this order parameter close to the percolation transition from either side of it is relatively well studied.

This study is dedicated to coupling of the physical effect of Casimir force between the two two-dimensional conducting sheets to the percolation transition in one of the sheets. Casimir force is the interaction between current fluctuations on the surface of conductors, leading to a force of, depending on exact geometry, attraction or repulsion at small distances between the interacting objects.

The percolation phenomenon occurs in the sheet independently of the Casimir interaction and defines the geometry of the interacting objects. Casimir interaction are in general not additive and depend on the whole geometry rather than on the sum of its parts. The geometry of the interacting objects defines the modes of the electric current oscillations that are possible on the surface of the conductors. The percolation phenomenon on the metal plate creates connected clusters of different finite sizes. The linear size of a cluster restricts the maximal wavelength of a current excitation that can exist on it. For this reason we expect that the magnitude of the Casimir force would differ depending on whether the infinite-wavelength current excitations are possible, which depends on the percolation phenomenon.

The question that this paper is trying to ask is whether there is a notable discontinuity or a phase transition in magnitude of the Casimir force between the two parallel plates as one of the plates passes the percolation threshold. To answer this question, the rest of the paper will proceed as follows.

Chapter 2 discusses a specific simple kind of the percolation phenomenon percolation - site percolation on a two-dimensional triangular lattice. The percolation threshold for that system is known exactly, as well as the near-critical behavior. Chapter 3 provides more theoretical background on Casimir effect. Chapter 4 provides a literature review for other systems in which some kind of a percolation transition affect the magnitude of the Casimir force. Chapter 5 describes the system that we would study numerically as well as the review of the computational method. Chapter 6 discusses results of the simulations and their statistical interpretations. Chapter 7 gives conclusions of our work and the directions of further study.

II. PERCOLATION ON 2D LATTICES

The particular system that exhibits the percolation transition is the plane triangular lattice. We would use reference [1] to analyse this system to find the exact percolation threshold by the series matching method.

A plane is laid out by triangles, and the focus of our attention is on the nodes. Each node is colored independently into black with probability p or white with probability $q = 1 - p$. We denote the bonds between two black nodes as black nodes and the bonds between two wide nodes as white bonds. Bonds between black and white nodes are denoted as uncolored. An example of realization of this system is given by Fig. 1.

We define a black cluster as a group of black nodes and bonds that are interconnected with each other and are completely surrounded by white nodes. For a given realization of percolation it is possible to count the number of black clusters. As percolation probability is increased, the number of black clusters growth. At some critical probability the number of black clusters experiences a singularity, which corresponds to the percolation transition. On the other side, we can consider the high-density limit, in which the white nodes form clusters within the uniform black matrix. The expression for the number of

* miflynn@mit.edu

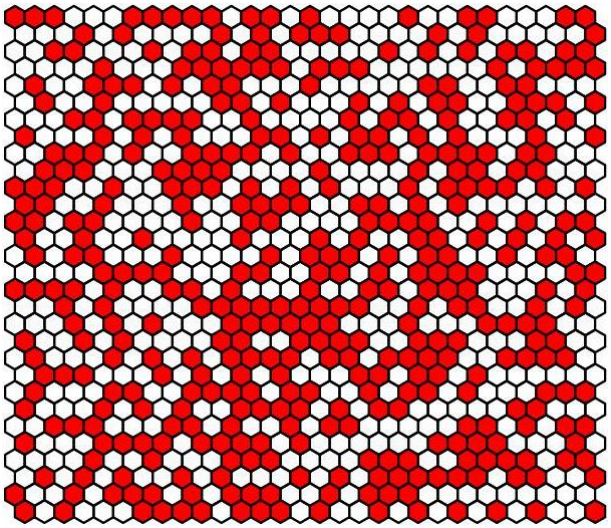

FIG. 1. An example realization of the triangular bond percolation at $p = 0.5$. In this illustration each node is replaced with a hexagon for visualization purposes. Each hexagon has 6 neighbours, thus this system is topologically equivalent to the triangular lattice percolation.

white clusters would be equivalent to the expression for the number of black clusters under the exchange $p \leftrightarrow q$.

To determine the percolation threshold, we need to calculate the average number of clusters. We do so by summing over all types of connected clusters in order of increasing complexity. The term corresponding to each type of cluster requires all the nodes of the cluster to be black and all the neighbors to be white. Thus clusters of the higher order of complexity correspond to the terms of higher orders in p and q. As well, there are several ways to orient each type of cluster - so, one of the simplest types of clusters consisting of just two joined nodes can be oriented three ways on a triangular lattice. Additionally, all types of clusters can be independently placed in any place of the N lattice sites (ignoring boundary effects). The factor of N would enter every single term of the number of clusters series and thus cannot contribute to their singularity. We define $k_b(p)$ as the mean number of clusters per site:

$$k(p,q) = K(p,q)/N \tag{1}$$

The series for $k(p,q)$ is given by the sum over clusters of increasing complexity [**?**]:

$$\begin{aligned} k_b(p) = pq^6 + 3p^2q^8 + p^3(2q^9 + 9q^{10}) \\ + p^4(3q^{10} + 12q^{11} + 29q^{12}) + O(p^5) \end{aligned} \tag{2}$$

To do the comparison of the series expansions we replace this two-parameter cluster expansion with the one-parameter expansions by setting $q = 1 - p$. From the duality considerations $k_b(p) = k(p, 1-p)$, $k_w(q) = k(1-q, q)$, from symmetry $k_b(p) = k_w(1-q)$. Now we comparatively examine the shapes of the expansions k_b and k_w by assigning them the same argument.

$$\begin{aligned} k_b(p) =& p - 3p^2 + 2p^3 + p^6 - p^7 + 3p^8 - 4p^9 + 9p^{10} - 15p^{11} + O(p^{12}) \\ k_w(p) =& \qquad\qquad p^6 - p^7 + 3p^8 - 4p^9 + 9p^{10} - 15p^{11} + O(p^{12}) \end{aligned} \tag{3}$$

From the comparison of these two series we find that the difference between them is a finite-order polynomial:

$$k_b(p) = \phi(p) + k_w(p) \tag{4}$$

The function $\phi(p)$ is a finite-order polynomial, thus it cannot have a singularity. Also we know that $k_b(p) = k_w(1-p)$, thus they would experience singularity simultaneously. The only value of p at which the equation 4 would hold with singularity on both sides is if $p_c = 0.5$. As well, the polynomial $\phi(p_c) = 0$, so the equation becomes an exact equality of two singular series.

III. CASIMIR EFFECT

The Casimir effect was originally described as a generalization of the van der Waals force between induced dipoles where the separation would be so large compared to the extent of the dipoles that the finite speed of light would need to be accounted for. The analysis of this particular problem was simplified by considering conducting plates of infinite area instead of point dipoles, leading to the idea that the Casimir effect may be evidence of a quantum vacuum electromagnetic energy. That said, this simplification depended on the assumption that the conductor was perfect, which requires that the fine structure constant could be considered as arbitrarily large compared to the inverse refraction index and the inverse square of the plate separation; alternatively, the plasma frequency of the metal would have to be arbitrarily large so that the metal would be opaque to all frequencies [2]. Thus, the notion that the Casimir effect fundamentally arises from a quantum electromagnetic vacuum can be cast away.

Instead, it is more useful to consider the Casimir effect as in fact a generalization of the van der Waals force. Atoms and molecules in any macroscopic material body can form temporary dipole moments due to fluctuations

arising from quantum uncertainty in position; this remains true even at zero temperature, ensuring that thermal considerations cannot be the sole cause of dipole fluctuations. When these fluctuating dipoles arise, they radiate electromagnetic fields outward, and these fields interact with and scatter from fluctuating dipoles in the same as well as other macroscopic bodies, as radiated fields can propagate over long spatial ranges. By accounting for the radiated electric field from an isolated fluctuating dipole, the dipole can be seen to effectively interact with itself from the scattering of its radiated field by other dipoles [3]. The radiated fields from a fluctuating dipole as well as the scattering from other dipoles can be calculated classically as long as the dipoles themselves are treated quantum mechanically, so the problem of determining Casimir interactions reduces to a classical electromagnetic scattering problem. As a brief example, it is useful to consider how the fluctuating current viewpoint of the Casimir effect can qualitatively (and quantitatively as well, through more technical arguments) reproduce the attraction of large neutral conducting plates suspended in a vacuum. The conducting plates are both filled with fluctuating dipoles which radiate in all directions. Radiation in the directions away from the plates cannot affect dipoles on the plates anymore, and as electromagnetic fields carry momentum, the opposite impulse would push each plate toward the other. Radiation from each plate in the directions toward the other plate can be absorbed and reradiated by dipoles on the other plate, and this would push the given plate away from the other plate; this comparison is most relevant for the longest wavelengths, because the dipoles and conductivity enforce effective boundary conditions that suppress the ability of dipoles on one plate to radiate at long wavelengths to dipoles on the other plate compared to directions away from the plates. Overall, then, long-wavelength radiation has more opportunities to leave the plates entirely than to go between the plates, so the plates are pushed together.

More generally and formally, two microscopic currents in a body are correlated in position and frequency at zero temperature due to quantum fluctuations by

$$\langle J_i(\omega,\mathbf{x})J_j^\star(\omega,\mathbf{x}')\rangle = \frac{\hbar\omega}{2\pi}\sigma(\omega,\mathbf{x})\delta_{ij}\delta(\mathbf{x}-\mathbf{x}') \tag{5}$$

given complex current densities $\mathbf{J}(\mathbf{x},\omega)$, where the index i denotes the Cartesian vector component. Here $\frac{\hbar\omega}{2}$ arises from the Planck distribution at zero temperature which is the ground state energy of a quantum harmonic oscillator, and $\sigma(\omega,\mathbf{x})$ arises because currents produce electric fields that induce other currents through the conductivity σ. This implies that currents at different positions are uncorrelated, and currents in different directions are uncorrelated as it is energetically favorable for electric fields to align with dipoles. For any configuration of material bodies, $G_{ij}^{(\mathbf{E})}(\omega,\mathbf{x},\mathbf{x}')$ and $G_{ij}^{(\mathbf{H})}(\omega,\mathbf{x},\mathbf{x}')$ are the relations of the fields $\mathbf{E}(\omega,\mathbf{X})$ and $\mathbf{H}(\omega,\mathbf{x})$, respectively, to point dipole sources at position $\mathbf{x}'$ oscillating at frequency ω. This yields

$$E_i(\omega,\mathbf{x}) = \int G_{ij}^{(\mathbf{E})}(\omega,\mathbf{x},\mathbf{x}')J_j(\omega,\mathbf{x}')\,d^3x' \tag{6}$$

$$H_i(\omega,\mathbf{x}) = \int G_{ij}^{(\mathbf{H})}(\omega,\mathbf{x},\mathbf{x}')J_j(\omega,\mathbf{x}')\,d^3x' \tag{7}$$

for the fields from general current distributions, where sums over repeated indices are implicit and will remain so throughout this section. Using the current autocorrelation in conjunction with these Green's function relations, along with the electromagnetic Green's function identities [4]

$$\int G_{ik}^{(\mathbf{E})}(\omega,\mathbf{x},\mathbf{x}'')G_{jk}^{\star(\mathbf{E})}(\omega,\mathbf{x}',\mathbf{x}'')\sigma(\omega,\mathbf{x}'')\,d^3x'' = \frac{1}{\omega}\mathrm{Im}(G_{ij}^{(\mathbf{E})}(\omega,\mathbf{x},\mathbf{x}')) \tag{8}$$

$$\int G_{ik}^{(\mathbf{H})}(\omega,\mathbf{x},\mathbf{x}'')G_{jk}^{\star(\mathbf{H})}(\omega,\mathbf{x}',\mathbf{x}'')\sigma(\omega,\mathbf{x}'')\,d^3x'' = \frac{1}{\omega}\mathrm{Im}(G_{ij}^{(\mathbf{H})}(\omega,\mathbf{x},\mathbf{x}')) \tag{9}$$

yields

$$\langle E_i(\omega,\mathbf{x})E_j^\star(\omega,\mathbf{x}')\rangle = \frac{\hbar}{2}\mathrm{Im}(G_{ij}^{(\mathbf{E})}(\omega,\mathbf{x},\mathbf{x}') \tag{10}$$

$$\langle H_i(\omega,\mathbf{x})H_j^\star(\omega,\mathbf{x}')\rangle = \frac{\hbar}{2}\mathrm{Im}(G_{ij}^{(\mathbf{H})}(\omega,\mathbf{x},\mathbf{x}') \tag{11}$$

as the correlation of the respective electromagnetic fields between different spatial positions due to fluctuating currents at zero temperature. As the Casimir force per unit frequency

$$\mathcal{F}_i(\omega) = \int T_{ij}(\omega,\mathbf{x})dS_j \tag{12}$$

arises from the Maxwell stress tensor

$$T_{ij} = E_iE_j + H_iH_j - \frac{\delta_{ij}}{2}(\mathbf{E}^2+\mathbf{H}^2) \tag{13}$$

which describes the flux of momentum in direction i along direction j, then

$$\mathcal{F}_i(\omega) = \frac{\hbar\omega}{\pi}\mathrm{Im}\left(\int\left(\mathcal{G}_{ij}^{(\mathbf{E})}(\omega,\mathbf{x},\mathbf{x}') + \mathcal{G}_{ij}^{(\mathbf{H})}(\omega,\mathbf{x},\mathbf{x}') - \frac{\delta_{ij}}{2}\left(\mathcal{G}_{kk}^{(\mathbf{E})}(\omega,\mathbf{x},\mathbf{x}') + \mathcal{G}_{kk}^{(\mathbf{H})}(\omega,\mathbf{x},\mathbf{x}')\right)\right)dS_j\right) \tag{14}$$

is the Casimir force per unit frequency in terms of the scattering Green's functions $\mathcal{G}$, which are the parts of G that do not arise from dipoles at the position $\mathbf{x}$ causing fields at the same position $\mathbf{x}$. This quantity can be integrated over the full range of frequencies to yield the total Casimir force

$$F_i = \int_0^\infty \mathcal{F}_i(\omega)\,d\omega \tag{15}$$

which is the quantity of interest for the rest of this paper.

Embedded in the Green's functions is information about the boundary conditions of the problem, which include the boundaries between different dielectric and conducting regions. Because the total Casimir force integrates over the entire range of frequencies, the behavior of the Casimir force is purely dependent on the parameters of the system geometry. Because percolation is a phenomenon of critical behavior purely through geometry, this makes examining the relationship between the Casimir force and percolation transitions a natural next step to take. In particular, it is useful to consider mixtures of metal and dielectric materials on a large sheet interacting with a pure metal sheet, where the mixed sheet is said to percolate if the largest connected component of metal grows as a constant fraction of the overall sheet size. Because long-wavelength electromagnetic modes are most relevant to the Casimir force especially at large plate separations, and because the field boundary conditions are far stronger for metal interfaces than dielectric interfaces, then at large plate separations, it would be reasonable to expect that the Casimir force would be related to whether or not the plate percolates. In particular, it may be reasonable to expect that when the mixed sheet percolates, as it looks more like a pure metal sheet from afar, then the Casimir force would behave more like that of the pure metal sheet; inverting this, when the mixed sheet does not percolate, then it looks more like a pure dielectric sheet from afar, so the Casimir force might behave more like that of a pure dielectric sheet. That said, the percolation probability will depend on the linear size of the giant connected component and the size of said component will be an areal size, whereas the radiation pressures in effect for the Casimir force depend much more on the relative areas of metal and dielectric components. Thus, it is not entirely clear just from this conceptual perspective that the Casimir force should transition in behavior at exactly the same point as a percolation transition, so a fuller theoretical analysis is required.

IV. EFFECTIVE MEDIUM THEORY AND PERCOLATION-CASIMIR RELATION

Near a percolation transition, where cluster sizes follow a characteristic power-law distribution, and indeed at all values of the site removal probability p for the finite lattices considered below, the highly inhomogeneous nature of the composite medium is unavoidable and must be properly accounted for in any theoretical treatment. Analytical investigation of its bulk dielectric or conductive properties, which is needed to predict the dependence of the Casimir force on p, filling fraction, or any other parameter that induces a percolation transition at some critical value, generally necessitates an approach known as the *effective medium approximation* (EMA). This technique is best illustrated by example. We adapt the canonical model given by Stroud [6] and introduced by the originators of EMA, Bruggeman and Landauer: a 2D mixture of two types A and B of circular grains, having conductivities σ_A and σ_B and occupying area fractions p and $1-p$ respectively, which we wish to approximate as a homogeneous medium with effective conductivity σ_e in which every grain is embedded. From electrostatics we obtain an expression for the internal electric field

$$E = E_0 \frac{2\sigma_e}{\sigma_{A/B} + \sigma_e}$$

in grains of type A/B where E_0 is the average field, giving a self-consistency condition

$$\begin{aligned} E_0 &= pE_0 \frac{2\sigma_e}{\sigma_A + \sigma_e} + (1-p)E_0 \frac{2\sigma_e}{\sigma_B + \sigma_e} \\ \implies 0 &= p\frac{\sigma_A - \sigma_e}{\sigma_A + \sigma_e} + (1-p)\frac{\sigma_B - \sigma_e}{\sigma_B + \sigma_e}. \end{aligned} \tag{16}$$

The special case of σ_A finite and $\sigma_B = 0$ (a metal-insulator mixture) can easily be seen to give the singular behavior

$$\sigma_e = \begin{cases} 0 & p < p_c \\ 2\sigma_A(p - p_c) & p > p_c \end{cases}$$

for the effective bulk conductivity near $p_c = 1/2$. It can be seen that this coincides with the site percolation threshold previously discussed in II for a triangular lattice, which is indeed the configuration that gives the greatest packing density for circular grains in 2D.

Unsurprisingly, the effective medium approach is adopted more or less universally in the literature by the few existing treatments of systems in which the Casimir force exhibits interesting or qualitatively different behavior near a percolation transition. We address three of them in turn before moving on to the percolation transition of interest in our investigation.

The first, considered by Sun et al. [8], is a generalization of the three-dimensional analogue of the toy model considered above, with parallel half-space in which metallic and dielectric grains with respective permittivities ϵ_1 and ϵ_2 are randomly distributed at filling fractions f and $1-f$. Their model allows for metallic grains that are not strictly spherical but instead ellipsoids characterized by a "depolarization factor" L_z such that $0 < L_z < 1/3$ indicates a prolate spheroid, $L_z = 1/3$ a perfect sphere, and $1/3 < L_z < 1$ an oblate spheroid. From this, a generalized EMA gives an implicit equation for the effective permittivity ϵ_e analogous to (though obviously more complicated than) (16) for σ_e, from which an L_z-dependent percolation threshold

$$f_c = \frac{9L_z(1-L_z)}{-9L_z^2 + 15L_z + 2}. \tag{17}$$

can be derived. In [8] it is reported that at constant metallic filling fraction f the normalized Casimir force $\eta = F/F_C$ attains a minimum for the spherical case $L_z = 1/3$. Furthermore, as shown in Fig. 2, the inflection point of η as a function of f at a fixed L_z (that is the maximum of $d\eta/df$) exactly coincides with the percolation threshold f_c given by (17).

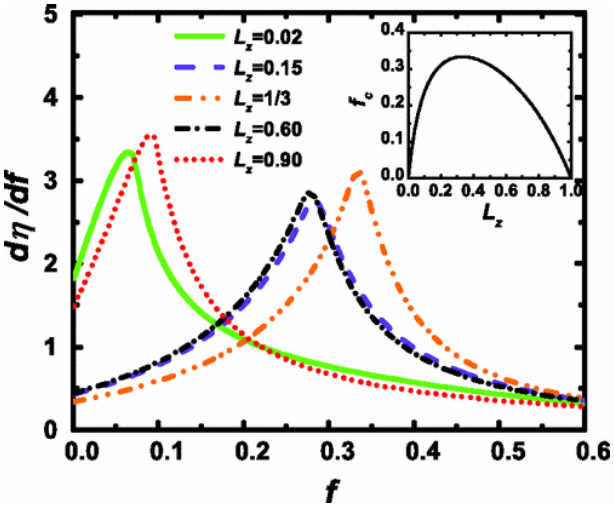

FIG. 2. Derivative of the normalized Casimir force η versus filling fraction f for a range of values for depolarization factor L_z in **??**, each displaying a sharp maximum coinciding with the percolation value f_c.

Our other two examples of a Casimir-percolation relation from the literature concern a transition less amenable to a direct effective-medium treatment than Sun et al.'s, but more similar to our own in dimensionality and physical realization: the metal-insulator transition in thin films and 2D plates. In [7], Esquivel-Sirvent addresses the behavior of the Casimir force between a half-space of pure gold and an Au thin film deposited on an Si substrate in the neighborhood of the latter's metal-insulator transition as a function of varying thickness. This transition coincides with a percolation threshold because deviations from the average thickness result in interpenetrating conducting and insulating regions, roughly delineated by a thickness comparable to the electron mean free path. Using Lifshitz's generalization of Casimir's original derivation, relating the force between the surfaces to their optical properties via the fluctuation-dissipation relation, as well as experimental terahertz spectroscopy data due to Walther, Esquivel-Sirvent finds that the minimum of the normalized Casimir force η coincides with this transition (see Fig. 3). Below the percolation threshold d_c, η rises slowly with decreasing thickness in the insulating regime, but the increase is much sharper in the conducting regime $d > d_c$.

Similarly, Galkina et al. in [9] apply the same Lifshitz theory to so-called "poor metals" comprising inhomogeneous composites of metals and dielectrics in 2D

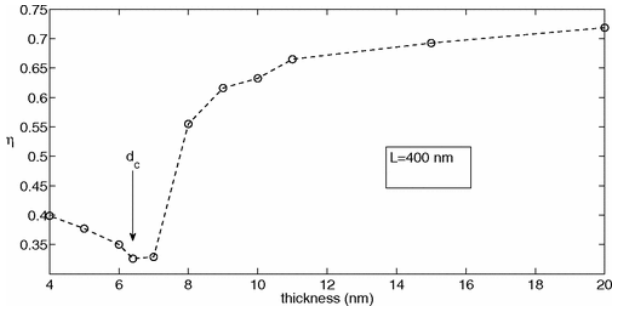

FIG. 3. Normalized Casimir force η as a function of Au thin film thickness d, showing a clear minimum coinciding with the metal-insulator percolation transition at d_c.

plates, which lend themselves well to an effective-medium analysis. In their model the metal-insulator transition is driven by variation of temperature rather than thickness, though it too can be characterized in the vicinity of its critical value T_c as a percolation transition. In the neighborhood of T_c they find (similarly to d_c in [7]) that η rises sharply by a factor of 2 or more on the conducting side, though they observe no increase with $|T - T_c|$ on the insulating one.

A review of the existing literature on the relation between Casimir-force behavior and three different realizations of a metal-dielectric percolation transition thus gives no clear picture of the expected behavior for our model. The percolation threshold f_c in filling fraction of ellipsoidal metallic inclusions in 3D slabs marks an inflection point in normalized Casimir force η as a function of f; the threshold value d_c for Au thin film thickness coincides with a (highly asymmetrical) minimum of η with a much steeper rise on the conducting side; and the critical temperature T_c for a bulk metal-insulator transition in a "poor metal" distinguishes a constant η on the insulating side from a sharp rise and plateau on the conducting one. None of these three extant examples should *a priori* be especially instructive for the system we consider, which if anything is closest in spirit to the two-component 2D toy model addressed at the beginning of this section (though the last of the three is probably closest). Indeed, the percolation transition we address is reached in a fashion topologically equivalent to site removal in a triangular lattice. As further detailed in the next section, we instead punch out individual cells with probability p in a square lattice with every other row offset by a half side-length, as shown in Fig. 4. Due to the previously established result that percolation occurs for triangular-lattice site removal at $p_c = 1/2$, the topological equivalence leads us to expect a transition at the same value in our exact model.

V. NUMERICAL METHODS FOR CASIMIR FORCES AND DATA

Our analysis makes use of the Electromagnetic Scattering codes developed by Dr. Homer Reid, collectively entitled SCUFF-EM. These codes use the boundary-element method of classical electrodynamics to carry out numerical calculations of various physical quantities, including equilibrium Casimir forces. In particular, we make use of the SCUFF-CAS3D suite of codes, which carries out Casimir computations for compact, three-dimensional objects. Given a configuration of objects, the Casimir energy of the configuration and the force on any of the objects are given, respectively, by

$$\mathcal{E} = \frac{\hbar}{2\pi}\int_0^\infty d\xi \log\frac{\det M(\xi)}{\det M_\infty(\xi)} \tag{18}$$

$$\mathcal{F}_i = -\frac{\hbar}{2\pi}\int_0^\infty d\xi \,\mathrm{Tr}\left[M^{-1}(\xi)\cdot\frac{\partial M(\xi)}{\partial r_i}\right] \tag{19}$$

where M is the Boundary Element Method (BEM) matrix constructed for the system under consideration. Models of the geometries upon which these calculations are performed are constructed in Gmsh, a program which generates three-dimensional "meshes" of the objects in question [10]. Gmsh breaks the geometry into many small pieces (triangles) upon which individual BEM calculations can be carried out. Then by summing over the triangles on an object, numerical estimates of Casimir quantities are obtained. A mesh file of the model we will study is presented in figure (4)).

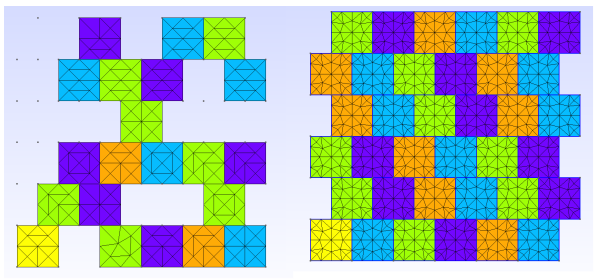

FIG. 4. A solid 6x6, meshed lattice is placed on the right with its hole-punched counterpart on the left. This generic skewed lattice geometry, where each row is staggered with respect to the previous row, forms the basis for the models we will consider. Each colored square represents a block of perfect conductor, while the triangles drawn on them were generated by gmsh for our numerical work.

As previously mentioned, the idea of removing squares of conductor to introduce a percolation transition is interesting due to its potential consequences for Casimir behavior. In practice, issues arise during the process of meshing objects which connect to each other at a single point. For example, removing only the nearest neighbors of a particular site on the square lattice leaves that site with neighbors at each of its corners, connecting to the site at a single point. This prevents gmsh from generating a "continuous" mesh across the surface, which is a restriction built into the mesh generator. Physically, this inability to mesh across point-like regions represents the fact that surface currents are not free to flow through arbitrarily tight channels.

These difficulties regarding the mesh process motivate us to introduce the skewed lattice of Figure 4. By inspection, it is clear that there is no way to remove any set of sites from the skewed lattice such that point like connections are introduced. This allows for an investigation of the effects of skewed lattice percolation on Casimir forces when the skewed lattice serves as a participant in the Casimir interaction. Further, as previously discussed, the percolation properties of the skewed lattice are quite convenient, as the process of removing squares is equivalent to site percolation on the triangular lattice.

Our data collection process involves the construction and implementation of several simulations involving perfect conductors. Initially, a 6x6 skewed lattice is produced, and to each of the 36 sites we assign an independent probability p of removing the site. Using SCUFF-CAS3D, this hole-poked lattice is placed parallel to the XY plane, centered on the z-axis with $z = 1$. A solid 6x6 skewed lattice is placed at the origin centered along the z-axis. With this configuration, the total Casimir energy and the Casimir force on each plate are computed via the BEM. This process is repeated as the hole-poked lattice is moved to various locations along the z-axis. Further, this series of calculations is done several times for each value of p in order to obtain a reasonable estimate of the expected value for the force and energy for that value of p.

VI. RESULTS AND DISCUSSION

The results of the force calculation are plotted in figure 5 for five values of p. For each p value, several hole-punched geometries were created and used in the calculation process, then averaged together. These averaged force values are plotted in figure 5, normalized at each point by the value of the force for $p = 0.5$. This data suggests that two types of long-distance behavior appear as a function of p. For $p > p_c = \frac{1}{2}$, more conducting pieces are removed from the material and it looks asymptotically like an insulator. For $p < p_c$, the plate is primarily a conductor, and more long-distance current fluctuations are present on the conductor, which gives rise to stronger long-range forces.

Unfortunately, time and computational constraints have prevented us from exploring a wider range of p values and separations. Our claims regarding the asymptotic behavior of the forces would be better substantiated by examining larger distances and using a solid plate ($p = 0$) for our normalization factor. However, the long-

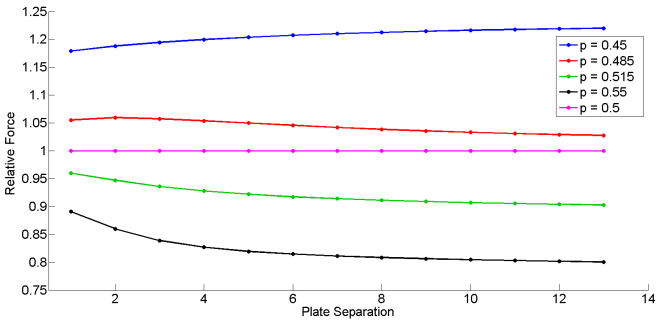

FIG. 5.

distance behavior seems to split at $p_c = \frac{1}{2}$ in the data collected, and this corresponds to the expected critical percolation probability. Taking steps to control for finite size effects by implementing a larger lattice should also help to determine whether the critical splitting occurs at $p = \frac{1}{2}$.

VII. CONCLUSIONS

A number of important aspects of Casimir physics and percolation were explored. The fluctuating surface current interpretation of the Casimir effect lead us to consider how percolation of currents on conductors could impact Casimir behavior. By implementing the SCUFF-CAS3D code, we found numerical evidence that suggests percolation effects could be important to Casimir behavior.

Unfortunately, there are a number of confounding effects which would need to be eliminated in order to confirm that percolation is responsible for the results we have obtained. We were only able to consider 110 geometries overall, which needs to be increased in order to confirm that the averaging process is stable. Further, the set of percolation patterns we can observe is limited by considering a 6x6 lattice. Increasing the size of this lattice could lead to more interesting results, though this has the drawback of dramatically increasing the size of the BEM matrix and driving up the cost of computation. It remains to be seen whether or not a feasible algorithm can be constructed which could offset the computational cost of a larger lattice.

Overall, we cannot claim that percolation is primarily responsible for the data we have collected. Finite size effects make it difficult to tell if percolation is as important as the filling fraction of the conductor in question. Hence, an ideal test of the importance of percolation versus filling fraction would come from implementing periodic boundary conditions on the skewed lattice. Appropriate construction of the unit cell under these boundary conditions could settle the point more definitively than our data has been able to.

ACKNOWLEDGEMENTS

The authors would like to thank Dr. Homer Reid for the helpful discussions and free use of his code. Numerical computations were performed using SCUFF-EM, a free, open-source software implementation of the boundary-element method. The authors would also like to thank Professor Mehran Kardar for all the statistical physics he has taught us in the last year. Lastly, we would like to thank Miren Bamforth for her assistance with the necessary scripts.

[1] M. F. Sykesand J. W. Essam, "Exact Critical Percolation Probabilities for Site and Bond Problems in Two Dimensions", Journal of Mathematical Physics 5, 1117 (1964); doi: 10.1063/1.1704215
[2] R. L. Jaffe, e-print arXiv:hep-th/0503158
[3] Alejandro W. Rodriguez, Federico Capasso & Steven G. Johnson, "The Casimir effect in microstructured geometries", Nature Photonics 5, 211221 (2011), doi:10.1038/nphoton.2011.39
[4] Stefan Yoshi Buhmann, Dirk-Gunnar Welsch, e-print arXiv:quant-ph/0608118
[5] M. T. Homer Reid, Alejandro W. Rodriguez, and Steven G. Johnson, "Fluctuation-Induced Phenomena in Nanoscale Systems: Harnessing the Power of Noise", Proceedings of the IEEE, Vol. 101, No. 2, February 2013
[6] D. Stroud, "The effective medium approximations: Some recent developments", Superlattices and Microstructures, Volume 23, Issues 3-4, March 1998, Pages 567573, http://dx.doi.org/10.1006/spmi.1997.0524
[7] R. Esquivel-Sirvent, "Casimir force calculations near the insulator-conductor transition in gold thin films", Phys. Rev. A 77, 042107 - Published 11 April 2008
[8] J. Sun, X. K. Hua, A. V. Goncharenko, and L. Gao, "Casimir force between composite materials containing nonspherical particles", Phys. Rev. A 87, 042509 - Published 16 April 2013
[9] E. G. Galkina, B. A. Ivanov, Sergey Savelev, V. A. Yampolskii, and Franco Nori, "Drastic change of the Casimir force at the metal-insulator transition", Phys. Rev. B 80, 125119 - Published 22 September 2009
[10] C. Geuzaine and J.-F. Remacle. Gmsh: a three-dimensional finite element mesh generator with built-in pre- and post-processing facilities. International Journal for Numerical Methods in Engineering 79(11), pp. 1309-1331, 2009